




Article

Ab Initio Approach to the Structure, Vibrational Properties, and Electron Binding Energies of H₂S⋯SO₂

 Isaac O. M. Magalhães ¹, Benedito J. C. Cabral ^{1,2} and João B. L. Martins ^{1,*}
¹ Computational Chemistry Laboratory, Institute of Chemistry, University of Brasilia, Brasilia 70910900, DF, Brazil; isaac.magalhaes@aluno.unb.br (I.O.M.M.); bjcabral@fc.ul.pt (B.J.C.C.)

² Biosystems and Integrative Sciences Institute, BioISI, Faculdade de Ciências de Lisboa, 1749-016 Lisboa, Portugal

* Correspondence: lopes@unb.br

Abstract: The present study employs high-level ab initio calculations to investigate the structure, vibrational frequencies, and electronic properties of H₂S⋯SO₂. The analysis of vibrational frequencies reveals an intramolecular vibrational energy transfer phenomenon, where energy from the stretching modes of H₂S is transferred to the ν_{1s} mode of SO₂. At the CCSD(T)/aug-cc-pVQZ level, the interaction energy between H₂S and SO₂ is predicted to be 2.78 kcal/mol. Electron propagator theory calculations yield a HOMO–LUMO gap of 8.24 eV for H₂S⋯SO₂. Furthermore, by utilizing ab initio results for the adiabatic ionization energy and electron affinity, the electrophilicity of H₂S⋯SO₂ is estimated to be 2.01 eV. This value is similar to the electrophilicity of SO₂, suggesting comparable reactivity and chemical behavior. The non-covalent interaction (NCI) analysis of the H₂S⋯SO₂ complex emphasizes the significant contribution of non-covalent van der Waals interactions in its energetic stabilization.

Keywords: vibrational spectroscopy; CCSD(T); H₂S–SO₂ complex



Citation: Magalhães, I.O.M.; Cabral, B.J.C.; Martins, J.B.L. Ab Initio Approach to the Structure, Vibrational Properties, and Electron Binding Energies of H₂S⋯SO₂. *Molecules* **2023**, *28*, 6656. <https://doi.org/10.3390/molecules28186656>

Academic Editor: Ángel Martín Pendás

Received: 22 August 2023

Revised: 7 September 2023

Accepted: 14 September 2023

Published: 16 September 2023

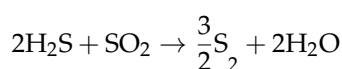
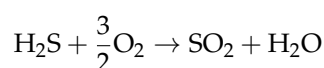


Copyright: © 2023 by the authors. Licensee MDPI, Basel, Switzerland. This article is an open access article distributed under the terms and conditions of the Creative Commons Attribution (CC BY) license (<https://creativecommons.org/licenses/by/4.0/>).

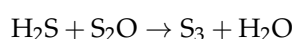
1. Introduction

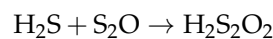
Acid rain is a significant environmental concern that has been widely studied and discussed. It is caused by the release of sulfur dioxide (SO₂) and other acidic pollutants into the atmosphere, which react with water vapor to form sulfuric acid (H₂SO₄) and other acids [1–7]. The natural pH of rain is close to 5.5. However, acid rain has a substantially lower pH, reaching 4.4. The low pH of this type of rain can cause structural problems in buildings and severe environmental damage, especially in primarily aquatic ecosystems [8].

Among the main sources of sulfur dioxide are industrial processes of burning fossil fuels. Sulfur organic and inorganic compounds are present in fossil fuels, with almost 3% of sulfur by weight [9]. However, sulfur supply comes from the desulfurization of fossil fuels of about 80%, which reduces the SO₂ emission [10–13]. Volcanoes, power plants, smelters, and the oil and gas industry are the primary sources of SO₂ [14]. H₂S primary emission comes from organic matter in swamp areas [15,16]. Processes involving desulfurization reactions, such as the Claus reaction, are used to convert sulfur-based gases, such as H₂S and SO₂, into elemental sulfur. The reaction typically proceeds as follows:



where the first reaction consists of the oxidation of H₂S to SO₂ and the second reaction is a gaseous reaction between H₂S and SO₂ to form the expected product. However, the second reaction can be processed to form S₂O and H₂O so that two new side reactions can start to occur [17]:





It is relevant to point out the greater facility presented by thiosulfurous acid to move to the $\text{H}_2\text{S}\cdots\text{SO}_2$ reagents, contrary to what would be expected to move to $\text{H}_2\text{O}\cdots\text{S}_2\text{O}$ [17].

In view of this problem, it becomes crucial to gain a comprehensive understanding of the interaction between H_2S and SO_2 as well as the associated energetics involved in forming the $\text{H}_2\text{S}\cdots\text{SO}_2$ complex. This understanding is particularly significant due to the influence of $\text{H}_2\text{S}\cdots\text{SO}_2$ in atmospheric chemistry and industrial contexts [17].

Applying methods developed in theoretical chemistry enables a comprehensive analysis of the structure and energetics of molecular systems, relying on a fundamental understanding of intermolecular interactions [18–22]. In the case of $\text{H}_2\text{S}\cdots\text{SO}_2$, there is evidence suggesting that the interactions occurring in this system are primarily associated with $\text{S}\cdots\text{S}$ chalcogen–chalcogen interactions [23–26]. These interactions play a crucial role in determining the stability and behavior of the $\text{H}_2\text{S}\cdots\text{SO}_2$ complex, highlighting the significance of studying these specific intermolecular interactions at a molecular level.

Post–Hartree–Fock computational chemistry methods, such as second-order Møller–Plesset Perturbation Theory (MP2), can be employed to investigate dimers of $\text{H}_2\text{S}\cdots\text{H}_2\text{S}$, $\text{SO}_2\cdots\text{SO}_2$, and $\text{H}_2\text{S}\cdots\text{SO}_2$. These methods allow for determining interaction energies and the distribution of electronic density [21,27]. On the other hand, CCSD(T) (Coupled Cluster with Single and Double excitations and Triple excitations corrections) can be utilized to obtain data related to the transfer of electron density between atoms, as well as the energies involved in the process and the geometry of the system. Notably, a high degree of accuracy is observed in the calculated energies when compared with experimental data [21,23,28]. An example is the recently reported results for $\text{H}_2\text{S}\cdots\text{H}_2\text{S}$, where CCSD(T) results agree with the geometry and vibrational frequencies [21]. These computational methods provide valuable insights into the electronic structure, energetics, and geometries of $\text{H}_2\text{S}\cdots\text{H}_2\text{S}$, $\text{SO}_2\cdots\text{SO}_2$, and $\text{H}_2\text{S}\cdots\text{SO}_2$ dimers, aiding in the understanding of their properties and behavior.

Another important aspect relates to the electronic properties of $\text{H}_2\text{S}\cdots\text{SO}_2$, particularly the energies of the frontier orbitals. These frontier orbitals play a significant role in ionization and electron attachment processes. By studying the energies of these orbitals, valuable information can be obtained regarding the reactivity and chemical behavior of the $\text{H}_2\text{S}\cdots\text{SO}_2$ system. Understanding the electronic properties and the energetics of the frontier orbitals provides insights into the potential for ionization or electron attachment events, which are relevant for various chemical and environmental processes involving $\text{H}_2\text{S}\cdots\text{SO}_2$. In this context, electron propagator theory (EPT) is reliable for obtaining accurate orbital energies. A detailed review on the methodology and applications of EPT was provided by Ortiz [29].

The focus of the present study is to accurately determine the structure, interaction energy, and electronic properties of the $\text{H}_2\text{S}\cdots\text{SO}_2$ system. This aim is achieved by employing high-level ab initio methods, specifically CCSD(T) and EPT. Some emphasis was placed on the calculation of reactivity indexes such as the chemical potential, hardness, and electrophilicity, which are closely related to the ionization and electron attachment processes [30].

2. Results and Discussion

2.1. Structure, Vibrational Frequencies, and Rotational Constants

2.1.1. Structure

The structure of $\text{H}_2\text{S}\cdots\text{SO}_2$ is illustrated in Figure 1. The complex is stabilized by SS chalcogen–chalcogen interaction. Additional $\text{O}\cdots\text{H}$ interactions should also be considered. The $\text{O}\cdots\text{H}$ distances observed in $\text{H}_2\text{S}\cdots\text{SO}_2$ are in the range of approximately 3.1–3.3 Å, as shown in Table 1. These distances fall on the upper side of the typical hydrogen bond range, which is generally between 2.3–3.3 Å.

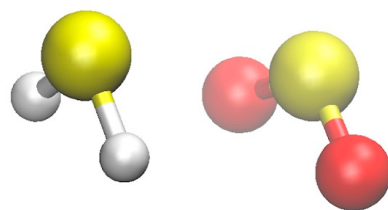


Figure 1. Structure of $\text{H}_2\text{S}\cdots\text{SO}_2$.

Table 1. Structure of $\text{H}_2\text{S}\cdots\text{SO}_2$: intermolecular distances (Å) and angles (degrees).

	S...S	H...O	OS...S	HS...S	θ	ϕ
MP2/AVTZ	3.414	3.107	89.27	76.78	88.623	70.768
MP2/AVQZ	3.387	3.137	90.11	78.40	90.215	73.140
MP2/AV5Z	3.382	3.156	90.33	79.24	90.615	74.288
CCSD/AVTZ	3.499	3.315	90.48	81.83	90.619	77.391
CCSD/AVQZ	3.481	3.335	90.70	82.37	91.324	78.983
CCSDT/AVTZ	3.454	3.181	89.25	78.43	88.558	73.168
CCSDT/AVQZ	3.427	3.221	90.12	80.33	90.248	75.960
Other Values						
Matsumura (a)	3.520	3.145			99.0(13)	56.8(11)
Kukolich (b)	3.45(1)				103(1)	71(3)
Ford (c)	3.802		72.88	67.28		
Plumer (d)	3.577	3.07				

(a) Experimental [31]; (b) Experimental [26]; (c) MP2/6-311G++(d,p) [23]; (d) MP2/6-31G* [27].

Intermolecular distances and angular parameters for $\text{H}_2\text{S}\cdots\text{SO}_2$ relying on different methods and basis sets are gathered in Table 1. Additional data for geometric parameters are reported in the Supplementary Material Tables S1–S3.

A comparison of optimized geometries at different theoretical levels and basis sets reveals that, in general, they are similar. Specifically, when using the AVQZ basis set, the predicted S...S distance differs by less than 0.06 Å between CCSD(T) and CCSD calculations. For the same basis set, a slight increase of approximately 0.2 Å in the O...H distance is observed when moving from MP2 to CCSD, although MP2 and CCSD(T) calculations yield similar values for this distance.

In general, a very good agreement is observed between theoretical and experimental data for the S...S distance. The CCSD(T)/AVTZ result for the S...S distance closely reproduces the experimental data reported by Kukolich et al. [26].

The angular parameters OS...S and HS...S in Table 1 show a maximum variation of 1.98 degrees for both HSH and OSO. The angles θ and ϕ , as defined in the work by Kukolich et al. [26], are also reported. θ represents the angle between the SO_2 plane and the SS line, while ϕ represents the angle between the H_2S plane and the SS line. Our calculated values of angle θ are smaller than the experimental values reported by Kukolich et al. [26]. One possible explanation is that their values were obtained through a fitting procedure involving rotational constants and different fittings were proposed in their work [26].

When comparing the structural parameters of the H_2S and SO_2 fragments with those in $\text{H}_2\text{S}\cdots\text{SO}_2$, it is observed that most of the changes in bond lengths and valence angles are primarily associated with the SO_2 fragment. The SO_2 fragment exhibits more significant changes in distances and angles compared with the relatively smaller changes observed in H_2S .

The data obtained in MP2 calculations indicate that the variations in bond lengths for H-S bonding in the $\text{H}_2\text{S}\cdots\text{SO}_2$ complex compared to the monomer values are smaller than 0.2%. Similarly, the variations in the HSH angle for H_2S in the complex are less than 0.3%. For the SO_2 fragment, the variations in bond lengths are below 0.08% and the angle variation is within 0.6% when comparing the complex to the monomer values. Indeed, the results obtained from MP2 calculations strongly suggest that the structural changes in the

H₂S⋯SO₂ complex, when compared to the isolated H₂S and SO₂ molecules, are minimal. This indicates that the interaction between H₂S and SO₂ does not significantly alter the overall geometry of the individual molecules. These findings provide valuable insights into the nature of the H₂S⋯SO₂ complex and its molecular behavior.

In the case of the CCSD(T) calculations, it is observed in Table 1 that the S⋯S interaction distance is smaller than in the MP2 and CCSD calculations. This result suggests that the excited triple correction provides a better description of dispersion interaction.

Table S3 shows the difference found in the H₂S⋯SO₂ complex regarding the monomer-optimized geometry. The difference in the interatomic distances is smaller than 0.0021 Å for the distances and 3.5° for the angles. In general, the interatomic distances show the same trend for all methods. The MP2 r(SH) and r(SO) are closer to the CCSD(T) values than CCSD. Both HS and SO distances are slightly increased (almost 0.001 Å) in relation to the monomer distance, except MP2/AVDZ for the SO distance. Therefore, both bonds have weakened.

Compared with the H₂S⋯H₂S complex, the H₂S⋯SO₂ complex has received much less attention in studies reported in the literature, and the geometry and energies have fewer estimates. Despite the minor variations in bond distances and angles concerning the 1990 experimental data of Kukolich [26], the results of all correlation-consistent basis sets show reliability and are in better accordance than the theoretical results of the literature. Therefore, comparing with the experimental bond distance and angles, the useful geometric data obtained with CCSD(T)/aug-cc-pVTZ and CCSD(T)/aug-cc-pVQZ are suitable estimates for this complex and can be taken as a reference calculation.

2.1.2. Vibrational Frequencies

Stretching frequencies of H₂S and SO₂ have a gap between symmetric (ν_{1s}) and anti-symmetric (ν_{1a}) modes. Here, for both HS and SO stretching, we will define a parameter δ as $\nu_{1a}-\nu_{1s}$ to represent the gap between the antisymmetric (ν_{1a}) and symmetric (ν_{1s}) stretching frequencies.

Therefore, the discussion on the vibrational frequencies will initially prioritize the δ parameter as it is a more sensitive measure for evaluating the accuracy of the calculated frequencies. We notice that theoretical frequencies are harmonic; thus, no scaling factor to consider anharmonic effects is used. Table 2 reports the difference between theoretical and experimental gaps for H₂S and SO₂. Vibrational frequencies (in cm⁻¹) for the antisymmetric ν_{1a} and symmetric ν_{1s} stretching modes in H₂S⋯SO₂ are reported in Supplementary Material Table S4.

Table 2. Difference between theoretical and experimental data for the antisymmetric–symmetric gap δ (in cm⁻¹) for the H₂S and SO₂ monomers.

	AVTZ	AVQZ	AV5Z
H ₂ S	$\delta_{th} - \delta_{expt}$	$\delta_{th} - \delta_{expt}$	$\delta_{th} - \delta_{expt}$
MP2	8.92	8.57	8.21
CCSD	4.19	3.56	
CCSD(T)	5.40	5.07	
SO ₂	$\delta_{th} - \delta_{expt}$	$\delta_{th} - \delta_{expt}$	$\delta_{th} - \delta_{expt}$
MP2	-4.59	2.39	8.15
CCSD	-17.96	-10.98	
CCSD(T)	-15.13	-7.40	

For H₂S, the deviations from experimental data are positive and relatively small, with values less than 10 cm⁻¹. The results obtained from the CCSD method show better agreement with the experimental values.

On the other hand, for SO₂, the vibrational results obtained from the MP2 method are in good agreement with the experimental data. However, the CCSD and CCSD(T) methods

underestimate the gap between the symmetric and antisymmetric stretching frequencies for SO₂. It should be observed that δ for SO₂ presents the most significant deviations from the experimental data. Among various other sources to enhance confidence, a possible explanation for the observed differences could be the importance of including additional *d* functions in the calculation for studying structures and frequencies involving sulfur atoms [32,33]. As reported in the literature, including extra *d* functions can improve the accuracy of the estimates and better capture the electronic behavior of sulfur-containing molecules [32–35].

Despite the aforementioned importance of including extra *d* functions for studying structures and frequencies involving sulfur atoms, it has generally been observed that there is good agreement between theory and experiment for the structure and vibrational frequencies of H₂S⋯SO₂. This agreement supports the accuracy of the currently employed ab initio methods in predicting the properties of these molecules. The impact of spin contamination regarding the formation of the H₂S⋯SO₂ complex has been explored. The multireference T1 diagnostic, as defined for the CCSD wave function, is the Frobenius norm [36] and is used to establish the single-reference quality. The T1 diagnostic of CCSD/aug-cc-pVQZ is less than 0.018, which suggests that a single reference is probably enough for this system (values smaller than 0.02). As an alternative, the percentage of the molecular total atomization energy (%TAE_e(T)) is of practical use to assess the nondynamic correlation and the reliability of single reference calculation [37,38]. For the aug-cc-pVQZ basis set, %TAE_e(T) is less than 4.3%, which leads to confidence in using a single reference [39].

The strength of the interactions between H₂S and SO₂ in H₂S⋯SO₂ can be related to the difference between the vibrational frequencies in the complex and monomers. Table 3 reports results for $\Delta\nu \equiv \nu_{\text{H}_2\text{S}-\text{SO}_2} - \nu_X$, where X = H₂S, SO₂.

Table 3. Difference $\Delta\nu$ for the antisymmetric and symmetric stretching frequencies between H₂S⋯SO₂ and monomers.

	MP2			CCSD		CCSD (T)	
	AVTZ	AVQZ	AV5Z	AVTZ	AVQZ	AVTZ	AVQZ
HS							
$\Delta\nu_{1a}$	−14.60	−16.05	−11.76	−3.74	−5.86	−7.06	−6.71
$\Delta\nu_{1s}$	−13.88	−15.43	−11.29	−3.31	−5.93	−6.79	−6.62
SO							
$\Delta\nu_{1a}$	−1.60	−3.02	−3.76	−6.12	−5.83	−5.50	−5.86
$\Delta\nu_{1s}$	5.80	5.20	4.47	1.34	1.68	1.34	1.68

In the case of H₂S, both the antisymmetric stretching frequency (ν_{1a}) and symmetric stretching frequency (ν_{1s}) are red-shifted in the complex compared to the monomer. The CCSD method predicts smaller values for these frequencies while MP2 yields larger values. Regarding SO₂, the antisymmetric stretching frequency (ν_{1a}) is also red-shifted in the complex. Interestingly, the symmetric stretching frequency (ν_{1s}) is blue-shifted, meaning it is shifted to higher frequencies compared to the monomer. The observed result suggests that an intramolecular vibrational energy transfer occurs upon complex formation [40,41]. This process involves the transfer of vibrational energy from the stretching modes of H₂S to the ν_{1s} mode of SO₂. Due to this energy transfer, the antisymmetric stretching frequency of H₂S undergoes a red-shift, while the symmetric stretching frequency of SO₂ experiences a blue-shift. This phenomenon highlights the dynamic interplay and energy exchange between the vibrational modes of the molecules within the H₂S⋯SO₂ complex.

2.2. Interaction Energies and Electronic Properties

The complex geometry was characterized as a minimum energy structure by calculating vibrational frequencies that were real and positive. The interaction energy ΔE_I between H_2S and SO_2 in $H_2S \cdots SO_2$ was computed using this minimum geometry and is defined as

$$\Delta E_I = E(H_2S) + E(SO_2) - E(H_2S \cdots SO_2)$$

where the energy of the fragments $E(H_2S)$ and $E(SO_2)$ are calculated at the geometry of the $H_2S \cdots SO_2$ complex. Basis set superposition errors (BSSE) due to finite basis set effects were corrected using the counterpoise (CP) method, where the energies of the fragments are calculated with the same basis set of $H_2S \cdots SO_2$. The corrected ΔE_I is represented as $\Delta E_I(CP)$ in Table 4.

Table 4. Interaction energies (kcal/mol) and S...S distances (Å) for the complexes.

	S...S	ΔE_I	BSSE	$\Delta E_I(CP)$
MP2/AVTZ	3.4142	3.2268	0.4757	2.7600
MP2/AVQZ	3.3866	3.1661	0.2333	2.9500
MP2/AV5Z	3.3822	3.1021	0.1205	3.0000
CCSD/AVTZ	3.4993	2.7071	0.3788	2.3400
CCSD/AVQZ	3.4805	2.6006	0.1558	2.4600
CCSD(T)/AVTZ	3.4543	3.0396	0.4473	2.6000
CCSD(T)/AVQZ	3.4275	2.9537	0.1831	2.7800

It is observed in Table 4 that the S...S distance decreases with the increase in the basis-set size. In parallel, the analysis of energies shows a more significant increase with the basis set. Our best result for the interaction energy $\Delta E_I(CP)$ is 2.78 kcal/mol from CCSD(T)/AVQZ. Excepting an MP2/6-31G* result reported by Plummer [27] for the binding energy of $H_2S \cdots SO_2$ of 1.7 kcal/mol, interaction energy data are apparently not available in the literature. In the absence of precise values for the interaction energy of $H_2S \cdots SO_2$, it is worth noting that a DFT study [42] reported an interaction energy of 5.86 kcal/mol for the $H_2O \cdots SO_2$ system. This finding predicts stronger binding energy compared to the $H_2S \cdots SO_2$ interaction, which is the expected result.

2.3. Electronic Properties

2.3.1. Electron Binding Energies and Reactivity Parameters

Table 5 reports the vertical and adiabatic ionization energies (IEs) and the electron affinities (EAs) of H_2S , SO_2 , and $H_2S \cdots SO_2$. $\Delta E(CCSD)$ calculations were performed to account for relaxation effects during ionization or electron attachment processes, predicting adiabatic IEs and EAs. The estimates include zero-point vibrational energy (ZPVE) corrections at the MP2/AVTZ level.

Table 5 presents the results obtained using different methods: Koopman's theorem (KT), outer valence Green's function (OVGF), and the partial third-order (P3) approximation. The results obtained from Koopman's theorem demonstrate the Hartree–Fock theory's predictive power and limitations. Compared with the EPT results, it becomes evident that electronic relaxation and correlation effects, which are absent in Hartree–Fock theory, play a significant role. In general, the OVGF approximation provides results that are in better agreement with experimental data. Therefore, the discussion of orbital energies will primarily focus on the results obtained from the OVGF approximation.

The calculated ionization energy (IE) of H_2S from the outer valence Green's function (OVGF) method, which is 10.448 eV, is in excellent agreement with the experimental value of 10.453 ± 0.008 eV. This IE corresponds to the highest occupied molecular orbital (HOMO) energy in H_2S . Furthermore, based on the results obtained for the electron affinities (EAs) of H_2S , no significant electron attachment is expected to occur for this species.

Recent Electron Propagator Theory (EPT) results for SO₂ were reported by Pawlowski and Ortiz [43]. Our calculations using the outer valence Green's function (OVGF) method yield very good agreement with their reported values and the experimental value of 12.349 eV [44]. The vertical and adiabatic ionization energies of SO₂ are 12.619 eV and 12.537 eV, respectively, which closely match their results of 12.614 eV and 12.427 eV. The electron affinity calculation places the LUMO energy of SO₂ at 0.73 eV, resulting in a HOMO–LUMO (HL) gap of 11.9 eV. The adiabatic electron affinity obtained from $\Delta E[\text{CCSD}]$ calculations is 1.267 eV, which is in good agreement with the experimental value of 1.14 ± 0.05 eV reported by Rothe in 1975 [45] and 1.107 ± 0.008 eV reported by Nimlos in 1986 [46].

Regarding H₂S–SO₂, the OVGF results for the vertical ionization energy and electron affinity are 10.619 eV and 0.609 eV, respectively, leading to a HOMO–LUMO gap of 8.24 eV. The corresponding adiabatic values from $\Delta E[\text{CCSD}]$ calculations are 9.873 eV and 1.637 eV. Unfortunately, we are not aware of any experimental results for the ionization energy and electron affinity of H₂S⋯SO₂.

Table 5. Ionization energies and electron affinities (in brackets). EPT/AVQZ calculations were carried out with CCSD/AVTZ-optimized geometries. Adiabatic values rely on CCSD/AVQZ//MP2/AVTZ calculations. Values in eV.

	Vertical			Adiabatic
	KT	OVGF	P3+	$\Delta E[\text{CCSD}]$
	IE [EA]	IE [EA]	IE [EA]	IE [EA]
H ₂ S (a)	10.487 [−0.682]	10.448 [−0.507]	10.328 [−0.485]	10.343 [−0.468]
SO ₂ (b)	13.560 [−0.069]	12.619 [0.730]	12.751 [0.792]	12.537 [1.267]
H ₂ S–SO ₂	10.144 [0.111]	10.129 [0.979]	9.929 [1.043]	9.873 [1.637]

(a) IE 10.453 ± 0.008 [47]. (b) VIE: 12.614 OVGF AIE 12.437 (D-CCSD) [43]. (b) AEA: 1.14 ± 0.05 [45].

Figure 2 depicts a representation of the HOMO and LUMO of H₂S–SO₂. The HOMO exhibits a localized S p-orbital primarily confined to the H₂S fragment. On the other hand, the complex structure of the LUMO demonstrates spatial delocalization and p–d orbital mixing, primarily involving the SO₂ moiety.

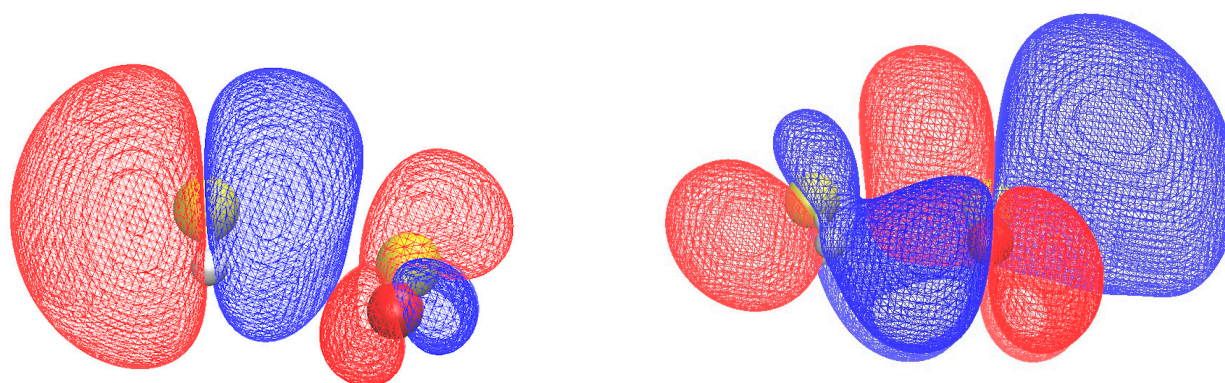


Figure 2. HOMO (left) and LUMO (right) of H₂S–SO₂. The isodensity is $0.005 (e/a_0^3)$.

A fundamental property for evaluating the affinity for electrons of a given species is its electrophilicity. However, unlike electron affinity (EA), which is concerned with the attachment of a single electron, electrophilicity assesses the energetic stabilization of a ligand in relation to the electron flow between donor and acceptor species [30].

The electrophilicity (ω) can be defined [30] as the relation between chemical potential and the global hardness:

$$\omega = \mu^2/2\eta$$

where the chemical potential μ and the chemical hardness η are given by

$$\mu = -(\text{IE} + \text{EA})/2 \quad \text{and} \quad \eta = (\text{IE} - \text{EA})/2$$

Table 6 reports the results for μ , η and ω , which are calculated using the CCSD/AVQZ//MP2/AVTZ values of ionization energies and electron affinities reported in Table 5. These reactivity descriptors are valuable in studying complex formation, where the maximum hardness principle correlates the largest hardness with the stability of a system [48,49].

Table 6. Chemical potential (μ), hardness (η), and electrophilicity (ω). Values in eV. Experimental values in brackets.

	$\mu = -\frac{\text{IE} + \text{EA}}{2}$	$\eta = \frac{\text{IE} - \text{EA}}{2}$	$\omega = \frac{\mu^2}{2\eta}$
H ₂ S	−4.937	5.406	2.255
SO ₂	−6.902	5.635	4.227 [4.027]
H ₂ S·SO ₂	−5.755	4.118	4.021

For SO₂ electrophilicity, the deviation from experimental results is less than 0.2 eV, indicating good agreement. Additionally, the electrophilicity value for H₂S·SO₂ (4.227 eV) is quite similar to the one predicted for SO₂, suggesting that the electron flow from the environment to H₂S·SO₂ is mainly determined by the SO₂ fragment. Fukui functions are depicted in Figure S1 and show the same trend of electrophilicity.

2.3.2. Electrostatic Potential and Non-Covalent Interactions (NCI) Analysis

Figure 3 presents the electrostatic potential (ESP) plotted on an isodensity surface for the H₂S·SO₂ complex (left panel) and the H₂O·SO₂ complex (right panel). In the case of H₂S·SO₂, the polarization effects arising from the difference between positive and negative regions of the electrostatic potential are primarily localized on the SO₂ monomer. This indicates that the interactions between H₂S and SO₂ predominantly involve the polarization of the SO₂ molecule. In contrast, for the H₂O·SO₂ complex, significant polarization effects are observed on both the H₂O and SO₂ monomers.

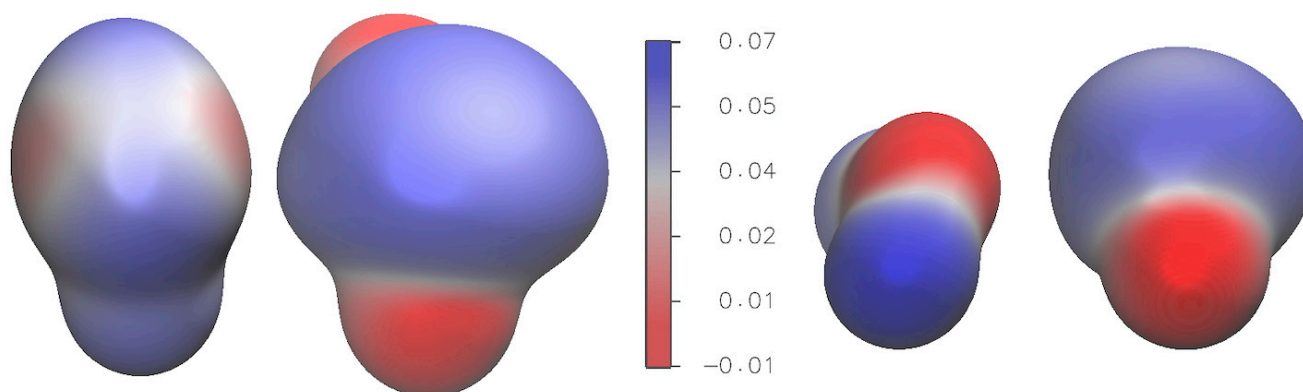


Figure 3. Electrostatic potential over isodensity surfaces. Left: H₂S·SO₂; right: H₂O·SO₂. The isodensity is 0.004 e/a₀³. Electrostatic potential in a.u.

One of the analyses utilized to characterize the nature of the interaction between two molecules is non-covalent interactions (NCI) analysis [50], as described by Contreras-García et al. [51]. This analysis examines the interaction on the same surface and provides valuable insights into the non-covalent forces at play. The results of this analysis are presented in Figure 4, which showcases the specific characteristics and distribution of the non-covalent interactions between H₂S and SO₂ within the complex.

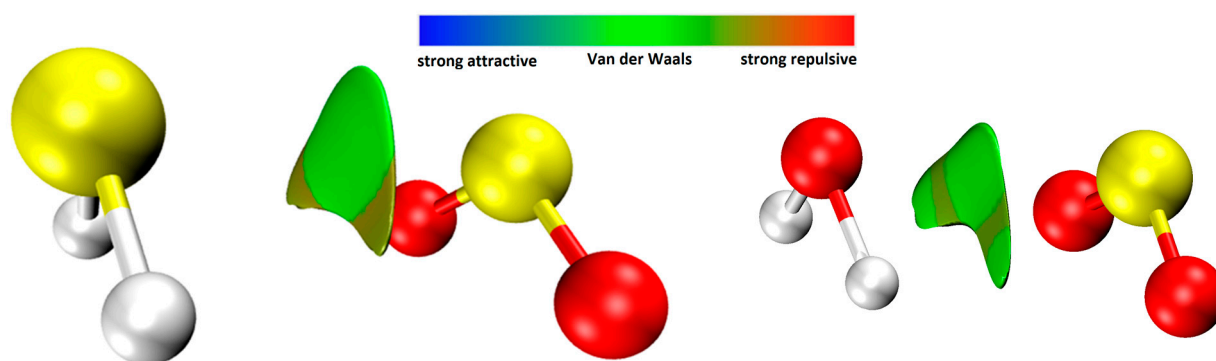


Figure 4. NCI analysis of the $\text{H}_2\text{S}\cdots\text{SO}_2$ interactions. Left: $\text{H}_2\text{S}\cdots\text{SO}_2$; right: $\text{H}_2\text{O}\cdots\text{SO}_2$. Color labels: yellow sulfur, red oxygen, and white hydrogen.

The NCI analysis depicted in Figure 4 highlights the significance of weak van der Waals interactions in energetically stabilizing the $\text{H}_2\text{S}\cdots\text{SO}_2$ complex. These interactions play a crucial role in the overall stability and binding of the complex. Additionally, the analysis reveals a depletion of electronic density between the fragments, indicating a characteristic feature of non-covalent interactions. It is important to note that there is also a presence of strong repulsion in certain regions of the same surface, as indicated by the brown region in Figure 4. This suggests the existence of repulsive forces between specific parts of the H_2S and SO_2 molecules within the complex. The interplay between attractive van der Waals interactions and repulsive forces contributes to the overall energetics and structural characteristics of the $\text{H}_2\text{S}\cdots\text{SO}_2$ complex. Interestingly, NCI analysis for the $\text{H}_2\text{O}\cdots\text{SO}_2$ complex also shows that non-covalent interactions play a significant role in the energetic stabilization of this system. This suggests that the natures of the intermolecular SS and SO interactions exhibit some similarity.

3. Materials and Methods

The structures of H_2S , SO_2 , and $\text{H}_2\text{S}\cdots\text{SO}_2$ were optimized using three different methods: MP2 (Møller–Plesset second-order perturbation theory) [52,53], CCSD (coupled cluster with single and double excitations) [54,55], and CCSD(T) (coupled cluster with single and double excitations, and correction to triple excitations) [56].

The MP2 and CCSD calculations were performed using the Gaussian16 program package [57]. On the other hand, the CCSD(T) calculation was carried out using the CFOUR program with analytical second derivatives [58].

To perform these calculations, three different levels of basis sets were used: aug-cc-pVTZ (AVTZ), aug-cc-pVQZ (AVQZ), and aug-cc-pV5Z (AV5Z). These basis sets are known as the Dunning correlation-consistent basis sets [59], and they provide increasingly accurate results including more basis functions from double-zeta to quintuple-zeta.

The use of monoelectronic basis sets in these calculations can lead to an overestimation of interaction energies due to the finite size of the basis sets and the different variational spaces of the complex ($\text{H}_2\text{S}\cdots\text{SO}_2$) and fragments (H_2S and SO_2). To address this issue, it is necessary to apply the Counterpoise (CP) correction method, which helps estimate the influence of the Basis Set Superposition Error (BSSE) [60]. The nature of the interaction between the H_2S and SO_2 monomers in $\text{H}_2\text{S}\cdots\text{SO}_2$ was discussed by non-covalent interactions (NCI) analysis [51].

Electron propagator theory (EPT) calculations were performed using the outer valence Green's function (OVGF) and partial third-order (P3) approximations [29]. EPT is known to provide accurate estimates of orbital energies. EPT calculations were carried out with the Gaussian16 program [28].

The adiabatic ionization energies and electron affinities were predicted through ΔE calculations, where the energy difference between the neutral and charged species was calculated. Optimized geometries for the neutral, cationic, and ionic species were determined

at the MP2/AVTZ level, and frequencies were calculated at the same level. Finally, energies were estimated at the CCSD/AVQZ//MP2/AVTZ level. Chemical reactivity indexes [30] were calculated using ionization energies and electron affinities from $\Delta E(\text{CCSD})$ calculations.

4. Conclusions

The present study employs high-level ab initio calculations to investigate the structure, vibrational frequencies, and electronic properties of the $\text{H}_2\text{S}\cdots\text{SO}_2$ complex. The analysis of vibrational frequencies reveals an intramolecular vibrational energy transfer phenomenon, where energy from the stretching modes of H_2S is transferred to the ν_{1s} mode of SO_2 . At the CCSD(T)/aug-cc-AVQZ level, the interaction energy between H_2S and SO_2 is predicted to be 2.78 kcal/mol. This provides insight into the strength of the interaction and the stability of the complex.

Electron propagator theory calculations yield a HOMO–LUMO gap of 8.24 eV for $\text{H}_2\text{S}\cdots\text{SO}_2$. This information sheds light on the electronic properties and the energy required for ionization and electron attachment processes. Furthermore, by utilizing ab initio results for the adiabatic ionization energy and electron affinity, the electrophilicity of $\text{H}_2\text{S}\cdots\text{SO}_2$ is estimated to be 2.01 eV. This value is found to be similar to the electrophilicity of SO_2 , suggesting comparable reactivity and chemical behavior.

Overall, the combination of ab initio calculations and analysis provides valuable insights into the structure, vibrational dynamics, and electronic properties of the $\text{H}_2\text{S}\cdots\text{SO}_2$ complex, contributing to a deeper understanding of this system. The non-covalent interactions (NCI) analysis conducted on the $\text{H}_2\text{S}\cdots\text{SO}_2$ complex emphasizes the significant contribution of non-covalent van der Waals interactions in its energetic stabilization.

Supplementary Materials: The following supporting information can be downloaded at: <https://www.mdpi.com/article/10.3390/molecules28186656/s1>, Figure S1: Fukui functions plotted for the complex using CCSD(T)/aug-cc-pVQZ; Table S1: Interatomic distances (Å) and bond angles (degrees) in the $\text{H}_2\text{S}\cdots\text{SO}_2$ complex; Table S2: Angles (degrees) in SO_2 , H_2S and in the $\text{SO}_2\cdots\text{H}_2\text{S}$ complex, where θ and φ are defined as in Ref [10]; Table S3: Difference of bond distances and angles of H_2S and SO_2 in relation to the monomer; Table S4: Vibrational frequencies (in cm^{-1}) for the antisymmetric ν_{1a} and symmetric ν_{1s} stretching modes in $\text{H}_2\text{S}\cdots\text{SO}_2$.

Author Contributions: Conceptualization, J.B.L.M. and B.J.C.C.; methodology, J.B.L.M. and B.J.C.C.; software, J.B.L.M. and I.O.M.M.; validation, J.B.L.M., I.O.M.M., and B.J.C.C.; formal analysis, J.B.L.M.; investigation, J.B.L.M.; resources, J.B.L.M.; data curation, J.B.L.M. and B.J.C.C.; writing—original draft preparation, J.B.L.M.; writing—review and editing, J.B.L.M. and B.J.C.C.; visualization, I.O.M.M.; supervision, J.B.L.M.; project administration, J.B.L.M.; funding acquisition, J.B.L.M. All authors have read and agreed to the published version of the manuscript.

Funding: This research was funded by Fundação de Amparo a Pesquisa do Distrito Federal (FAPDF), grant number 00193-00000869/2021-31.

Institutional Review Board Statement: Not applicable.

Informed Consent Statement: Not applicable.

Data Availability Statement: Data are available upon request.

Conflicts of Interest: The authors declare no conflict of interest.

Sample Availability: Not applicable.

References

1. Taieb, D.; Ben Brahim, A. Electrochemical Method for Sulphur Dioxide Removal from Flue Gases: Application on Sulphuric Acid Plant in Tunisia. *Comptes Rendus Chim.* **2013**, *16*, 39–50. [CrossRef]
2. Gerhard, E.R.; Johnstone, H.F. Air Pollution Studies—Photochemical Oxidation of Sulfur Dioxide in Air. *Ind. Eng. Chem.* **1955**, *47*, 972–976. [CrossRef]
3. Tewari, A.; Shukla, N.P. Air Pollution—Adverse Effects of Sulfur Dioxide. *Rev. Environ. Health* **1991**, *9*, 39–46. [CrossRef] [PubMed]
4. Ward, P.L. Sulfur Dioxide Initiates Global Climate Change in Four Ways. *Thin Solid Films* **2009**, *517*, 3188–3203. [CrossRef]

5. Johnstone, H.F.; Moll, A.J. Air Pollution by Formation of Sulfuric Acid in Fogs. *Ind. Eng. Chem.* **1960**, *52*, 861–863. [[CrossRef](#)]
6. Hoesly, R.M.; Smith, S.J.; Feng, L.; Klimont, Z.; Janssens-Maenhout, G.; Pitkanen, T.; Seibert, J.J.; Vu, L.; Andres, R.J.; Bolt, R.M.; et al. Historical (1750–2014) Anthropogenic Emissions of Reactive Gases and Aerosols from the Community Emissions Data System (CEDS). *Geosci. Model Dev.* **2018**, *11*, 369–408. [[CrossRef](#)]
7. Dignon, J.; Hameed, S. Global Emissions of Nitrogen and Sulfur Oxides from 1860 to 1980. *JAPCA* **1989**, *39*, 180–186. [[CrossRef](#)]
8. Clarke, A.G.; Radojevic, M. Oxidation of SO₂ in Rainwater and Its Role in Acid Rain Chemistry. *Atmos. Environ.* **1987**, *21*, 1115–1123. [[CrossRef](#)]
9. Speight, J.G. *8—Gas Cleaning Processes*, 2nd ed.; Gulf Professional Publishing: Boston, MA, USA, 2019; pp. 277–324. ISBN 978-0-12-809570-6.
10. Maslin, M.; Van Heerde, L.; Day, S. Sulfur: A Potential Resource Crisis That Could Stifle Green Technology and Threaten Food Security as the World Decarbonises. *Geogr. J.* **2022**, *188*, 498–505. [[CrossRef](#)]
11. Kato, N.; Akimoto, H. Anthropogenic Emissions of SO₂ and NO_x in Asia: Emission Inventories. *Atmos. Environ. Part A Gen. Top.* **1992**, *26*, 2997–3017. [[CrossRef](#)]
12. Klimont, Z.; Cofala, J.; Schöpp, W.; Amann, M.; Streets, D.G.; Ichikawa, Y.; Fujita, S. Projections of SO₂, NO_x, NH₃ and VOC Emissions in East Asia Up to 2030. *Water, Air, Soil Pollut.* **2001**, *130*, 193–198. [[CrossRef](#)]
13. Möller, D. Estimation of the Global Man-Made Sulphur Emission. *Atmos. Environ.* **1984**, *18*, 19–27. [[CrossRef](#)]
14. Fioletov, V.E.; McLinden, C.A.; Krotkov, N.; Li, C.; Joiner, J.; Theys, N.; Carn, S.; Moran, M.D. A Global Catalogue of Large SO₂ Sources and Emissions Derived from the Ozone Monitoring Instrument. *Atmos. Chem. Phys. Discuss.* **2016**, *16*, 11497–11519. [[CrossRef](#)]
15. Robinson, E.; Robbins, R.C. Gaseous Sulfur Pollutants from Urban and Natural Sources. *J. Air Pollut. Control Assoc.* **1970**, *20*, 233–235. [[CrossRef](#)]
16. Malone Rubright, S.L.; Pearce, L.L.; Peterson, J. Environmental Toxicology of Hydrogen Sulfide. *Nitric Oxide Biol. Chem.* **2017**, *71*, 1–13. [[CrossRef](#)] [[PubMed](#)]
17. Sendt, K.; Haynes, B.S. Role of the Direct Reaction H₂S + S₂O in the Homogeneous Claus Reaction. *J. Phys. Chem. A* **2005**, *109*, 8180–8186. [[CrossRef](#)]
18. Cunha, W.F.; Gargano, R.; Garcia, E.; Politi, J.R.S.; Albernaz, A.F.; Martins, J.B.L. Rovibrational Energy and Spectroscopic Constant Calculations of CH₄ Center Dot Center Dot Center Dot CH₄, CH₄ Center Dot Center Dot Center Dot H₂O, CH₄ Center Dot Center Dot Center Dot CHF₃, and H₂O Center Dot Center Dot Center Dot CHF₃ Dimers. *J. Mol. Model.* **2014**, *20*, 2298. [[CrossRef](#)]
19. de Menezes, R.F.; de Macedo, L.G.M.; Martins, J.B.L.; Pirani, F.; Gargano, R. Investigation of Strength and Nature of the Weak Intermolecular Bond in NH₂ Radical-Noble Gas Atom Adducts and Evaluation of Their Basic Spectroscopic Features. *Chem. Phys. Lett.* **2021**, *769*, 138386. [[CrossRef](#)]
20. Paura, E.N.C.; da Cunha, W.F.; Lopes Martins, J.B.; Magela e Silva, G.; Roncaratti, L.F.; Gargano, R. Carbon Dioxide Adsorption on Doped Boron Nitride Nanotubes. *RSC Adv.* **2014**, *4*, 28249–28258. [[CrossRef](#)]
21. Martins, J.B.L.; Quintino, R.P.; Politi, J.R.d.S.; Sethio, D.; Gargano, R.; Kraka, E. Computational Analysis of Vibrational Frequencies and Rovibrational Spectroscopic Constants of Hydrogen Sulfide Dimer Using MP2 and CCSD(T). *Spectrochim. Acta-Part A Mol. Biomol. Spectrosc.* **2020**, *239*, 118540. [[CrossRef](#)]
22. Politi, J.R.S.; Martins, J.B.L.; Cabral, B.J.C. Born-Oppenheimer Molecular Dynamics and Electronic Properties of Liquid H₂S: The Importance of a Non-Local Approach to Dispersion Interactions. *J. Mol. Liq.* **2022**, *366*, 120252. [[CrossRef](#)]
23. Ford, T.A. Ab Initio Molecular Orbital Calculations of the Structures and Vibrational Spectra of Some Molecular Complexes Containing Sulphur Dioxide. *J. Mol. Struct.* **2009**, *924–926*, 466–472. [[CrossRef](#)]
24. Pauley, D.J.; Bumgarner, R.E.; Kukolich, S.G. Microwave Spectrum of the SO₂-H₂S Complex. *Chem. Phys. Lett.* **1986**, *132*, 67–68. [[CrossRef](#)]
25. Bumgarner, R.E.; Pauley, D.J.; Kukolich, S.G. Microwave Spectra and Structure for SO₂⋯H₂S, SO₂⋯HDS, and SO₂⋯D₂S Complexes. *J. Chem. Phys.* **1987**, *87*, 3749–3752. [[CrossRef](#)]
26. Kukolich, S.G.; Pauley, D.J. Comment on: Structure of H₂S-SO₂. *J. Chem. Phys.* **1990**, *93*, 871–872. [[CrossRef](#)]
27. Plummer, P.L.M. Quantum-Mechanical Studies of Weakly-Bound Molecular Clusters. *J. Mol. Struct.* **1994**, *113*, 119–133. [[CrossRef](#)]
28. Lemke, K.H. Structure and Binding Energy of the H₂S Dimer at the CCSD (T) Complete Basis Set Limit. *J. Chem. Phys.* **2017**, *146*, 234301. [[CrossRef](#)]
29. Ortiz, J.V. Electron Propagator Theory: An Approach to Prediction and Interpretation in Quantum Chemistry. *WIREs Comput. Mol. Sci.* **2013**, *3*, 123–142. [[CrossRef](#)]
30. Parr, R.G.; Szentpály, L.v.; Liu, S. Electrophilicity Index. *J. Am. Chem. Soc.* **1999**, *121*, 1922–1924. [[CrossRef](#)]
31. Matsumura, K.; Lovas, F.J.; Suenram, R.D. The Microwave Spectrum and Structure of the H₂S-SO₂ Complex. *J. Chem. Phys.* **1989**, *91*, 5887–5894. [[CrossRef](#)]
32. Wilson, A.K.; Dunning, T.H., Jr. SO₂ Revisited: Impact of Tight d Augmented Correlation Consistent Basis Sets on Structure and Energetics. *J. Chem. Phys.* **2003**, *119*, 11712–11714. [[CrossRef](#)]
33. Wilson, A.K.; Dunning, T.H. The HSO-SOH Isomers Revisited: The Effect of Tight d Functions. *J. Phys. Chem. A* **2004**, *108*, 3129–3133. [[CrossRef](#)]
34. Wang, N.X.; Wilson, A.K. Effects of Basis Set Choice upon the Atomization Energy of the Second-Row Compounds SO₂, CCl, and ClO₂ for B3LYP and B3PW91. *J. Phys. Chem. A* **2003**, *107*, 6720–6724. [[CrossRef](#)]

35. Bell, R.D.; Wilson, A.K. SO₃ Revisited: Impact of Tight d Augmented Correlation Consistent Basis Sets on Atomization Energy and Structure. *Chem. Phys. Lett.* **2004**, *394*, 105–109. [[CrossRef](#)]
36. Lee, T.J.; Taylor, P.R. A Diagnostic for Determining the Quality of Single-Reference Electron Correlation Methods. *Int. J. Quantum Chem.* **1989**, *36*, 199–207. [[CrossRef](#)]
37. Karton, A.; Rabinovich, E.; Martin, J.M.L.; Ruscic, B. W4 Theory for Computational Thermochemistry: In Pursuit of Confident Sub-KJ/Mol Predictions. *J. Chem. Phys.* **2006**, *125*, 144108. [[CrossRef](#)]
38. Wang, J.; Manivasagam, S.; Wilson, A.K. Multireference Character for 4d Transition Metal-Containing Molecules. *J. Chem. Theory Comput.* **2015**, *11*, 5865–5872. [[CrossRef](#)]
39. Karton, A.; Daon, S.; Martin, J.M.L. W4-11: A High-Confidence Benchmark Dataset for Computational Thermochemistry Derived from First-Principles W4 Data. *Chem. Phys. Lett.* **2011**, *510*, 165–178. [[CrossRef](#)]
40. Uzer, T.; Miller, W.H. Theories of Intramolecular Vibrational Energy Transfer. *Phys. Rep.* **1991**, *199*, 73–146. [[CrossRef](#)]
41. Tardy, D.C.; Rabinovitch, B.S. Intermolecular Vibrational Energy Transfer in Thermal Unimolecular Systems. *Chem. Rev.* **1977**, *77*, 369–408. [[CrossRef](#)]
42. Venkataraman, N.S. Electronic Structure, Stability, and Cooperativity of Chalcogen Bonding in Sulfur Dioxide and Hydrated Sulfur Dioxide Clusters: A DFT Study and Wave Functional Analysis. *Struct. Chem.* **2022**, *33*, 179–193. [[CrossRef](#)]
43. Pawłowski, F.; Ortiz, J.V. Ionization Energies and Dyson Orbitals of the Iso-Electronic SO₂, O₃, and S₃ Molecules from Electron Propagator Calculations. *J. Phys. Chem. A* **2021**, *125*, 3664–3680. [[CrossRef](#)] [[PubMed](#)]
44. Wang, L.; Lee, Y.T.; Shirley, D.A. Molecular Beam Photoelectron Spectroscopy of SO₂: Geometry, Spectroscopy, and Dynamics of SO⁺₂. *J. Chem. Phys.* **1987**, *87*, 2489–2497. [[CrossRef](#)]
45. Rothe, E.W.; Tang, S.Y.; Reck, G.P. Measurement of Electron Affinities of O₃, SO₂, and SO₃ by Collisional Ionization. *J. Chem. Phys.* **1975**, *62*, 3829–3831. [[CrossRef](#)]
46. Nimlos, M.R.; Ellison, G.B. Photoelectron Spectroscopy of Sulfur-Containing Anions (SO₂⁻, S₃⁻, and S₂O⁻). *J. Phys. Chem.* **1986**, *90*, 2574–2580. [[CrossRef](#)]
47. Walters, E.A.; Blais, N.C. Molecular Beam Photoionization and Fragmentation of D₂S, (H₂S)₂, (D₂S)₂, and H₂S·H₂O. *J. Chem. Phys.* **1984**, *80*, 3501–3502. [[CrossRef](#)]
48. Parr, R.G.; Pearson, R.G. Absolute Hardness: Companion Parameter to Absolute Electronegativity. *J. Am. Chem. Soc.* **1983**, *105*, 7512–7516. [[CrossRef](#)]
49. Pearson, R.G. The Principle of Maximum Hardness. *Acc. Chem. Res.* **1993**, *26*, 250–255. [[CrossRef](#)]
50. Johnson, E.R.; Keinan, S.; Mori-Sánchez, P.; Contreras-García, J.; Cohen, A.J.; Yang, W. Revealing Noncovalent Interactions. *J. Am. Chem. Soc.* **2010**, *132*, 6498–6506. [[CrossRef](#)]
51. Contreras-García, J.; Johnson, E.R.; Keinan, S.; Chaudret, R.; Piquemal, J.-P.; Beratan, D.N.; Yang, W. NCIPLOT: A Program for Plotting Noncovalent Interaction Regions. *J. Chem. Theory Comput.* **2011**, *7*, 625–632. [[CrossRef](#)]
52. Head-Gordon, M.; Head-Gordon, T. Analytic MP2 Frequencies without Fifth-Order Storage. Theory and Application to Bifurcated Hydrogen Bonds in the Water Hexamer. *Chem. Phys. Lett.* **1994**, *220*, 122–128. [[CrossRef](#)]
53. Møller, C.; Plesset, M.S. Note on an Approximation Treatment for Many-Electron Systems. *Phys. Rev.* **1934**, *46*, 618–622. [[CrossRef](#)]
54. Scuseria, G.E.; Schaefer III, H.F. Is Coupled Cluster Singles and Doubles (CCSD) More Computationally Intensive than Quadratic Configuration Interaction (QCISD)? *J. Chem. Phys.* **1989**, *90*, 3700–3703. [[CrossRef](#)]
55. Hirata, S.; Podeszwa, R.; Tobita, M.; Bartlett, R.J. Coupled-Cluster Singles and Doubles for Extended Systems. *J. Chem. Phys.* **2004**, *120*, 2581–2592. [[CrossRef](#)] [[PubMed](#)]
56. Purvis III, G.D.; Bartlett, R.J. A Full Coupled-cluster Singles and Doubles Model: The Inclusion of Disconnected Triples. *J. Chem. Phys.* **1982**, *76*, 1910–1918. [[CrossRef](#)]
57. Frisch, M.J.; Trucks, G.W.; Schlegel, H.B.; Scuseria, G.E.; Robb, M.A.; Cheeseman, J.R.; Scalmani, G.; Barone, V.; Petersson, G.A.; Nakatsuji, H.; et al. *Gaussian 16, Revision C.01*; Gaussian Inc.: Wallingford, CT, USA, 2016.
58. Stanton, J.F.; Gauss, J.; Cheng, L.; Harding, M.E.; Matthews, D.A.; Szalay, P.G. CFOUR, Coupled-Cluster Techniques for Computational Chemistry, a Quantum-Chemical Program Package. *J. Chem. Phys.* **2020**, *152*, 214108.
59. Dunning, T.H., Jr. Gaussian Basis Sets for Use in Correlated Molecular Calculations. I. The Atoms Boron through Neon and Hydrogen. *J. Chem. Phys.* **1989**, *90*, 1007–1023. [[CrossRef](#)]
60. Mentel, Ł.M.; Baerends, E.J. Can the Counterpoise Correction for Basis Set Superposition Effect Be Justified? *J. Chem. Theory Comput.* **2014**, *10*, 252–267. [[CrossRef](#)]

Disclaimer/Publisher's Note: The statements, opinions and data contained in all publications are solely those of the individual author(s) and contributor(s) and not of MDPI and/or the editor(s). MDPI and/or the editor(s) disclaim responsibility for any injury to people or property resulting from any ideas, methods, instructions or products referred to in the content.